

Asymptotic methods for confined fluids

E. Di Bernardo and J. M. Brader

Department of Physics, University of Fribourg, CH-1700 Fribourg, Switzerland

The thermodynamics and microstructure of confined fluids with small particle number are best described using the canonical ensemble. However, practical calculations can usually only be performed in the grand-canonical ensemble, which can introduce unphysical artifacts. We employ the method of asymptotics to transform grand-canonical observables to the canonical ensemble, where the former can be conveniently obtained using the classical density functional theory of inhomogeneous fluids. By formulating the ensemble transformation as a contour integral in the complex fugacity plane we reveal the influence of the Yang-Lee zeros in determining the form and convergence properties of the asymptotic series. The theory is employed to develop expansions for the canonical partition function and the canonical one-body density. Numerical investigations are then performed using an exactly soluble one-dimensional model system of hard-rods.

I. INTRODUCTION

Statistical mechanical studies of classical equilibrium fluids are typically performed using the grand-canonical ensemble, where the average particle number in the system is controlled by the chemical potential of a particle reservoir. While this presents several technical advantages for calculation, there exist many situations in which particle number fluctuations induce unphysical errors and a canonical treatment would be preferable.

When can we expect differences between the grand-canonical and canonical ensembles to be relevant? The most obvious case is when the particle number is small, such that the system is far from the thermodynamic limit [1, 2]. Small systems are naturally associated with localization of the particles and thus a spatially inhomogeneous one-body density distribution. In the simplest case, small groups of particles can be localized by the application of a confining external potential field, for example hard-spheres in a cavity or harmonic confining potential [3, 4]. Alternatively, the localization may be a consequence of a mutual attraction between the particles, which binds them together in a finite size cluster [5]. If the bulk system exhibits an equilibrium phase transition, e.g. from a gas to a liquid, then the situation becomes more complicated and one has to consider more carefully how many particles constitute a ‘small number’. If the thermodynamic parameters are close to those of the bulk critical point, then even a confined fluid with many particles can exhibit finite-size effects due to the development of long-ranged correlations.

Localized systems with small particle number have a microstructure and thermodynamics which differs significantly from those of an infinite bulk system; interfacial effects become dominant. The most commonly employed and well studied framework for determining the equilibrium properties of inhomogeneous classical fluids is the Density Functional Theory (DFT) [6, 7]. This approach has proved enormously useful in the study of inhomogeneous fluids but exhibits grand-canonical artifacts in situations for which the particles are strongly localized [3, 4, 8, 9]. Although DFT has been formally recast in

the canonical ensemble [10, 11], the complexity of implementation has hindered its application to concrete problems. In the rare cases for which grand-canonical quantities are known exactly a matrix inversion scheme may be employed to obtain exact canonical information [8]. However, when the grand-canonical input is only approximately known, as is usually the case for models of interest, the method becomes unstable as errors in the grand-canonical input quantities become amplified.

An alternative, albeit approximate, route to obtaining canonical quantities was investigated by Salaceuse *et al.* [12], who expanded the canonical structure factor as a power series in N^{-1} , aiming to account for leading-order finite-size effects in simulation data. This approach, which builds upon early work of Lebowitz and Percus [13], was subsequently extended to inhomogeneous systems by González *et al.* to approximate the canonical one-body density profile [3, 4]. A second-order truncation of their expansion was shown to yield very good results for the density profile of hard-spheres in a hard spherical cavity. The key to the success of these methods lies in the rapid convergence of the partial sums of the series, since calculation of the higher-order coefficients soon becomes computationally demanding.

In this paper the transformation of observables from the grand-canonical to the canonical ensemble is formulated as a contour integral in the complex fugacity plane. From this starting point we use the method of steepest descents [14–16] to develop asymptotic expansions for both the canonical partition function and canonical one-body density profile, although extension to higher-order correlation functions would not pose any additional difficulties. Typical applications of steepest descents in the mathematical literature concern the approximate evaluation of intractable integrals for large values of a control parameter. Although the steps involved in constructing valid asymptotic series surely require much thought and subtlety, one at least knows the integrand as a closed-form analytic expression over the entire integration domain. When seeking to apply asymptotics to transform between ensembles we do not have this luxury. Grand-canonical observables can usually only be calculated (numerically) for positive real values of the fugacity, whereas

the contour integral for transforming to the canonical ensemble demands grand-canonical input calculated over the full complex fugacity plane. This limited knowledge of the integrand hinders determination of the optimal steepest descents contour. Careful consideration and ingenuity are thus required to find a contour capable of generating correctly the leading-order terms in the series, with the hope that fast convergence makes calculation of higher-order terms unnecessary.

Although the asymptotic method is approximate it can sometimes offer deeper insight into the essential elements of a physical problem than would be available from a complicated exact solution. In the present case we find that the asymptotic expansion of canonical quantities is intimately connected with the presence of singular points of the grand partition function in the complex fugacity plane: the famous Yang-Lee zeros. These nontrivial singularities play an important role in determining the optimal steepest-descents integration contour and therefore affect the convergence properties of the asymptotic series. Viewing the problem of ensemble transformation through the lens of asymptotics not only suggests new lines of attack but also sheds light on earlier studies in which the status of the approximations employed was not entirely clear. For example, asymptotics reveals the Yang-Lee related pitfalls which would surely be encountered when attempting to apply the expansion of González *et al.* to realistic model fluids exhibiting a phase transition. The approach developed here thus brings together in an intuitive way the fields of classical DFT, ensemble transformation and the Yang-Lee theory of phase transitions.

II. DENSITY FUNCTIONAL THEORY

The primary method for obtaining grand-canonical information about confined or localized systems is the classical density functional theory (DFT). The central object in DFT is the grand potential functional [6, 7]

$$\Omega[\rho] = \mathcal{F}[\rho] - \int d\mathbf{r}(\mu - V_{\text{ext}}(\mathbf{r}))\rho(\mathbf{r}), \quad (1)$$

where μ is the chemical potential and $V_{\text{ext}}(\mathbf{r})$ is the external potential. The Helmholtz free energy, \mathcal{F} , appearing on the right hand-side of equation (1) is here a grand-canonical quantity and not the true canonical Helmholtz free energy for a system of fixed particle number. The ideal gas and interaction contributions to \mathcal{F} can be separated according to $\mathcal{F} = \mathcal{F}^{\text{id}} + \mathcal{F}^{\text{exc}}$. The ideal gas term is given exactly by

$$\mathcal{F}^{\text{id}}[\rho] = k_B T \int d\mathbf{r} \rho(\mathbf{r}) (\ln(\rho(\mathbf{r})) - 1), \quad (2)$$

where $k_B T$ is the thermal energy and where the (physically irrelevant) thermal wavelength has been set equal to unity. The excess Helmholtz free energy functional, \mathcal{F}^{exc} , encodes the interparticle interactions and usually

has to be approximated. The grand potential satisfies the variational condition

$$\left. \frac{\delta \Omega[\rho]}{\delta \rho(\mathbf{r})} \right|_{\rho_{\text{eq}}} = 0, \quad (3)$$

which then generates the Euler-Lagrange equation for the equilibrium density

$$\rho_{\text{eq}}(\mathbf{r}) = e^{-\beta(V_{\text{ext}}(\mathbf{r}) - \mu - k_B T c^{(1)}(\mathbf{r}; [\rho_{\text{eq}}]))}. \quad (4)$$

The one-body direct correlation function is a functional of the one-body density and is defined by the derivative

$$c^{(1)}(\mathbf{r}; [\rho_{\text{eq}}]) = - \left. \frac{\delta \beta F^{\text{exc}}[\rho]}{\delta \rho(\mathbf{r})} \right|_{\rho_{\text{eq}}}. \quad (5)$$

Substitution of the equilibrium density profile into the functional (1) generates the thermodynamic grand potential, $\Omega_{\text{eq}} = \Omega[\rho_{\text{eq}}]$, which is related to the grand partition function, Ξ , via the standard relation $\Omega_{\text{eq}} = -k_B T \ln(\Xi)$. Note that we will henceforth drop the subscript, $\rho_{\text{eq}} \equiv \rho$, since we will deal solely with equilibrium systems.

III. CANONICAL PARTITION FUNCTIONS AND THERMODYNAMIC QUANTITIES

A. Exact forwards and backwards transforms

The grand-canonical partition function is defined as a weighted sum of the canonical partition functions, Z_N , according to

$$\Xi(\lambda) = 1 + \sum_{N=1}^{\infty} \lambda^N Z_N, \quad (6)$$

where the fugacity is related to the chemical potential by $\lambda = \exp(\beta\mu)$. If the number of particles which the system can accommodate is limited by the physical situation under consideration, e.g. particles confined within a closed cavity, then the sum in (6) can be truncated at a maximum value, $N = N_{\text{max}}$. The relation (6) is essentially a discrete Laplace transform of the canonical partition function (depending on the discrete index N) to the grand-canonical partition function (a function of the continuous variable μ). We will henceforth refer to this as the ‘forward’ transform.

The grand-canonical partition function contains all statistically relevant information about the equilibrium system. It should therefore be possible in principle to invert the transformation (6) to obtain Z_N from the grand partition function. In reference [8] it is shown that if Ξ is known at N_{max} distinct trial values of the fugacity, $\lambda_1 \cdots \lambda_{N_{\text{max}}}$, then equation (6) generates a set of algebraic equations for the unknown canonical partition functions, $Z_1 \cdots Z_{N_{\text{max}}}$. If the grand partition function is exact, then the canonical partition functions resulting from

solution of this system of equations are also exact, with values independent of the chosen trial fugacities. Unfortunately, this scheme is of limited applicability, since we are usually forced to employ approximations to the grand potential (and hence the partition function). This renders the algebraic inversion of (6) ambiguous, as the values obtained for the canonical partition functions become dependent upon the arbitrary choice of trial fugacities. The instability of direct numerical inversion of (6) is perhaps not surprising, given experience with established numerical Laplace inversion schemes (see e.g. [17]). It is thus worth searching for alternatives which are more robust for applications and which may provide a deeper level of insight.

Although only positive real values of λ yield a physically meaningful grand partition function, the polynomial sum in (6) remains a well-defined mathematical quantity for complex values of λ . The exact inverse (back) transform corresponding to equation (6) has appeared sporadically in the statistical mechanics literature at various points over the last century (see, e.g. [13, 18–20]) and requires knowledge of Ξ over the full complex fugacity plane. The back transform is given by the following contour integral

$$Z_N = \frac{1}{2\pi i} \oint_C d\lambda \frac{\Xi(\lambda)}{\lambda^{N+1}}, \quad (7)$$

where the contour C can be chosen arbitrarily, provided that it encloses the pole at $\lambda=0$. We note, however, that the contour-independence of Z_N is only guaranteed when Ξ is known exactly. The most familiar occurrence in statistical mechanics of an integral of this type is as part of the Darwin-Fowler derivation of the canonical ensemble [18, 21]. A short explanation of equation (7) is given in appendix A.

The easiest way to evaluate the back-transform (7) would appear to be direct integration around some convenient contour enclosing the origin. The simplest choice we can make is a circular path, parameterized according to $\lambda=r \exp(i\phi)$, where the value of r should be irrelevant for the outcome. The back-transform then reduces to

$$Z_N = \frac{1}{2\pi r^N} \int_0^{2\pi} d\phi \left(\Xi_R(r, \phi) \cos(N\phi) + \Xi_I(r, \phi) \sin(N\phi) \right), \quad (8)$$

where Ξ_R and Ξ_I are the real and imaginary parts of the grand partition function, respectively, and where we have used the fact that Z_N is real. Given some expression for Ξ , which can be either exact or approximate, equation (8) then generates a prediction for Z_N for any integer value of the particle number N . The catch, however, is that implementing this procedure requires knowledge of the complex-valued grand partition function for all values of λ around a circle of radius r in the complex plane; information which is typically not available. In practice we usually only have access to approximate information

about Ξ on the positive real axis of the complex λ plane. A systematic way to deal with this difficulty, and to hopefully get the most out of the limited information available, is to use the method of asymptotics to approximate the integral in (7) as a power series in N^{-1} . Although the asymptotic method is not exact it provides a route to unambiguous calculation of the canonical partition functions, even in cases for which Ξ is not known exactly.

B. Steepest-descents approximation

1. General considerations

Using the Cartesian representation of the complex fugacity, $\lambda = x + iy$, we begin by considering the behavior of the integrand in equation (7), namely

$$I(\lambda) = \frac{\Xi(\lambda)}{\lambda^{N+1}}, \quad (9)$$

along the positive real axis, $\lambda=x$. The definition (6) and the positivity of Z_N imply that $\Xi(x)$ is positive for $x>0$. The thermodynamic relation $\langle N \rangle = -\partial \Omega / \partial \mu$, where $\langle N \rangle$ is the average number of particles in the grand-canonical system, can be expressed in the alternative form

$$\langle N \rangle = \frac{x}{\Xi} \frac{\partial \Xi}{\partial x}. \quad (10)$$

Since for positive values of x both $\langle N \rangle$ and Ξ are positive, it follows that the derivative $\partial \Xi / \partial x > 0$. The grand partition function is thus a monotonically increasing function of x . As the function $1/x^{N+1}$ is a monotonically decreasing function of x we can conclude that the integrand $I(x)$ has a minimum, which we denote by x_0 , on the positive real axis. Both Ξ and $1/x^{N+1}$ are analytic functions of the fugacity; recall that Ξ is simply an integer-power polynomial in λ . Consequently, the integrand $I(\lambda)$ obeys the second-order Cauchy-Riemann condition [22]

$$\frac{\partial^2 I}{\partial x^2} + \frac{\partial^2 I}{\partial y^2} = 0. \quad (11)$$

Since x_0 is a minimum along the real axis, it follows that

$$\left. \frac{\partial^2 I}{\partial x^2} \right|_{x=x_0, y=0} > 0, \quad \left. \frac{\partial^2 I}{\partial y^2} \right|_{x=x_0, y=0} < 0, \quad (12)$$

namely that there is a maximum of $I(\lambda)$ in the y -direction, parallel to the imaginary axis, at the point $\lambda=x_0$. We have thus identified a saddle point at $\lambda=x_0$.

Using a simple rearrangement, equation (7) can be put into the following standard form

$$Z_N = \frac{1}{2\pi i} \oint_C d\lambda \frac{e^{Nf(\lambda)}}{\lambda}, \quad (13)$$

where we have defined

$$f(\lambda) = \frac{1}{N} \ln \Xi(\lambda) - \ln \lambda, \quad (14)$$

which is the negative of the reduced Helmholtz free energy per particle, namely

$$f = -\frac{\beta\mathcal{F}}{N}. \quad (15)$$

As previously mentioned, the Helmholtz free energy appearing in (15) is a grand-canonical quantity. By now treating N as a large parameter we can apply the method of steepest descents [14–16, 23, 24] to equation (13) and thus develop an asymptotic expansion of the canonical partition function in powers of N^{-1} . The saddle-point, x_0 , about which we wish to expand is easily located by solution of the equation $df(x)/dx=0$, where the derivative is taken along the real axis. This leads to the saddle condition

$$\left(x \frac{\partial}{\partial x} \Xi(\lambda)\right) \Big|_{\substack{x=x_0 \\ y=0}} = N \Xi(x_0). \quad (16)$$

Combining equation (16) with the relation (10) shows that the saddle condition implies

$$\langle N \rangle|_{x_0} = N, \quad (17)$$

namely that the fugacity at the saddle-point is that which sets the average number of particles in the grand-canonical system equal to the sharp particle number in the canonical system.

2. The optimal choice of contour

The next question concerns the best choice of contour passing through the saddle point. Since the only formal requirement of the back transform (7) is that the contour encloses the origin we have some freedom to optimize our choice to take best advantage of the available information, i.e. the values of Ξ along the positive real axis. In the following we assume that the function f is analytic, which will turn out to be true, except at isolated points.

Separating f into its real and imaginary parts, $f \equiv f_{\text{re}} + i f_{\text{im}}$, the directional derivatives in a direction given by a unit vector \mathbf{n} are

$$\frac{df_{\text{re}}}{ds} = \mathbf{n} \cdot \nabla f_{\text{re}}, \quad (18)$$

$$\frac{df_{\text{im}}}{ds} = \mathbf{n} \cdot \nabla f_{\text{im}}, \quad (19)$$

where ds is a line element along \mathbf{n} . If we make the specific choice $\mathbf{n} = \nabla f_{\text{re}} / |\nabla f_{\text{re}}|$, then we obtain the largest possible value for the right-hand side of (18), namely

$$\frac{df_{\text{re}}}{ds} = |\nabla f_{\text{re}}|. \quad (20)$$

from which we conclude that f_{re} changes most rapidly in the direction of ∇f_{re} . Equation (19) becomes

$$\frac{df_{\text{im}}}{ds} = \frac{\nabla f_{\text{re}} \cdot \nabla f_{\text{im}}}{|\nabla f_{\text{re}}|}. \quad (21)$$

The two Cauchy-Riemann conditions $\partial f_{\text{re}}/\partial x = \partial f_{\text{im}}/\partial y$ and $\partial f_{\text{re}}/\partial y = -\partial f_{\text{im}}/\partial x$ [22] can be combined into the single expression

$$\left(\frac{\partial f_{\text{re}}}{\partial x}\right) \left(\frac{\partial f_{\text{im}}}{\partial x}\right) + \left(\frac{\partial f_{\text{re}}}{\partial y}\right) \left(\frac{\partial f_{\text{im}}}{\partial y}\right) = 0, \quad (22)$$

which is simply the vectorial condition $\nabla f_{\text{re}} \cdot \nabla f_{\text{im}} = 0$. Using this result in equation (21) leads to

$$\frac{df_{\text{im}}}{ds} = 0. \quad (23)$$

We can thus conclude that along a contour with tangent parallel to ∇f_{re} the function f will have a constant imaginary part and a real part which exhibits the most rapid possible rate of change.

The above observations are very useful in evaluating (13). Deforming the contour into a path along which the imaginary part of the function $f \equiv f_{\text{re}} + i f_{\text{im}}$ remains constant enables us to factor out a complex exponential which would otherwise generate inconvenient oscillations in the integrand. This yields

$$Z_N = \frac{e^{iNf_{\text{im}}}}{2\pi i} \oint_{\mathcal{C}^*} d\lambda \frac{e^{Nf_{\text{re}}(\lambda)}}{\lambda}, \quad (24)$$

where \mathcal{C}^* indicates that we are integrating along a contour of constant f_{im} . Furthermore, if we demand that \mathcal{C}^* passes through the saddle point on the real axis, where $f_{\text{im}} = 0$, it follows that f_{im} is not simply constant, but equal to zero around the entire contour. Choosing the contour \mathcal{C}^* ensures that the real part of the integrand decreases as rapidly as possible from its value at the saddle point (‘steepest descent’) [16]. The challenge when implementing the steepest descents scheme is that determination of the optimal contour \mathcal{C}^* requires knowledge of f , and thus Ξ , over the entire complex λ plane, whereas standard statistical mechanical methods (such as DFT) can only provide information along the real axis. In the following we will show how to deal with this difficulty.

Without loss of generality we begin by expressing the complex fugacity λ in polar form

$$\lambda = r e^{i\phi}, \quad (25)$$

and then substitute this into the expression (6) to obtain

$$\Xi_\phi(r) = 1 + Z_1 r e^{i\phi} + Z_2 r^2 e^{2i\phi} + Z_3 r^3 e^{3i\phi} + \dots, \quad (26)$$

where we have introduced the convenient shorthand notation $\Xi_\phi(r) \equiv \Xi(r, \phi)$. Taylor expansion of the exponential functions and collecting powers of ϕ then yields

$$\begin{aligned} \Xi_\phi(r) = & (1 + rZ_1 + r^2Z_2 + r^3Z_3 + \dots) \\ & + i\phi (rZ_1 + 2r^2Z_2 + 3r^3Z_3 + \dots) \\ & + \frac{(i\phi)^2}{2} (rZ_1 + 4r^2Z_2 + 9r^3Z_3 + \dots) \\ & + \frac{(i\phi)^3}{6} (rZ_1 + 8r^2Z_2 + 27r^3Z_3 + \dots) \\ & + \dots \end{aligned} \quad (27)$$

Starting from equation (26) we observe that repeated application of the operator $r \frac{\partial}{\partial r}$ to the grand-canonical partition function (at zero phase-angle) generates

$$\left(r \frac{\partial}{\partial r}\right)^n \Xi_0(r) = \sum_{j=1}^{\infty} j^n r^j Z_j. \quad (28)$$

For $n=1$ equation (28) generates the coefficient of $i\phi$ in equation (27), $n=2$ generates the coefficient of $(i\phi)^2/2$ and so on. This enables us to write equation (27) in the more compact form

$$\begin{aligned} \Xi_\phi(r) = & \Xi_0(r) + i\phi \left(r \frac{\partial}{\partial r}\right) \Xi_0(r) + \frac{(i\phi)^2}{2} \left(r \frac{\partial}{\partial r}\right)^2 \Xi_0(r) \\ & + \frac{(i\phi)^3}{6} \left(r \frac{\partial}{\partial r}\right)^3 \Xi_0(r) + \dots, \end{aligned} \quad (29)$$

which can be formally resummed to obtain

$$\Xi_\phi(r) = \left(e^{i\phi r \frac{\partial}{\partial r}}\right) \Xi_0(r). \quad (30)$$

Equation (30) seems to us to be an interesting and general result, the derivation of which relies solely on the polynomial form of the grand partition function. It tells us that if we know $\Xi_0(r)$ and its derivatives at a point r on the positive real axis ($\phi=0$), then application of the exponential ‘rotation operator’ will generate the value of the grand partition function at any point on a circle of radius r in the complex λ plane.

Let us now investigate the terms appearing in the Taylor expansion (29). From the definition of the grand partition function it is straightforward to show that

$$\left(i\phi r \frac{\partial}{\partial r}\right)^n \Xi_0(r) = i\phi \langle N^n \rangle \Xi_0(r), \quad (31)$$

for $n=1, \dots, \infty$. We recall that for $\phi=0$ the radial coordinate r is simply the fugacity on the positive real axis and that $\langle \cdot \rangle$ indicates a grand-canonical average quantity calculated at this value of r . The Taylor series (29) can therefore be reexpressed as follows

$$\Xi_\phi(r) = \left(1 + i\phi \langle N \rangle + \frac{(i\phi)^2}{2} \langle N^2 \rangle + \frac{(i\phi)^3}{6} \langle N^3 \rangle + \dots\right) \Xi_0(r). \quad (32)$$

The contour we seek could in principle be determined using the following procedure: (i) Substitute the expansion (32) and polar form (25) into the definition of f to obtain

$$f_\phi(r) = \frac{1}{N} \ln(\Xi_\phi(r)) - \ln(re^{i\phi}), \quad (33)$$

where we follow the notation already adopted for the grand partition function. (ii) Set the imaginary part of $f_\phi(r)$ equal to zero and solve the resulting equation to find the function $r(\phi)$ which maps out the contour \mathcal{C}^* . Unfortunately, practical implementation of this scheme

proves both cumbersome and numerically delicate. When using DFT, $\Xi_0(r)$ is generated using an iterative numerical procedure and the finite-difference derivatives required to calculate the moments $\langle N^n \rangle$ decrease in accuracy as the value of n increases.

For these reasons we look instead for an *approximate* contour which is more convenient for practical calculations, but still sufficient to capture correctly the low-order terms in the asymptotic expansion. The simplest way to achieve this is to neglect particle number fluctuations by making the factorization approximation $\langle N^n \rangle \approx \langle N \rangle^n$. Within this approximation equation (32) becomes

$$\Xi_\phi(r) \approx \left(1 + i\phi \langle N \rangle + \frac{(i\phi \langle N \rangle)^2}{2} + \frac{(i\phi \langle N \rangle)^3}{6} + \dots\right) \Xi_0(r). \quad (34)$$

which can then easily be resummed to give the following simple formula

$$\Xi_\phi(r) \approx e^{i\phi \langle N \rangle} \Xi_0(r). \quad (35)$$

Substitution of (35) into (33) then gives

$$f_\phi(r) \approx \left(\frac{1}{N} \ln(\Xi_0(r)) - \ln(r)\right) + i\phi \left(\frac{\langle N \rangle}{N} - 1\right), \quad (36)$$

from which we identify a clear separation into real and imaginary parts. If we now choose the fugacity to be equal to that at the saddle point, $r = x_0$, then $\langle N \rangle = N$ and the imaginary part of (37) vanishes, leaving us with

$$f_\phi(x_0) \approx \frac{1}{N} \ln(\Xi_0(x_0)) - \ln(x_0), \quad (37)$$

which is a real function. We have thus demonstrated that *within the factorization approximation* a circular contour, parameterized by the phase-angle and passing through the saddle point, leads to a constant imaginary part of f and that the value of this constant is zero.

If we would not make the factorization approximation and use the exact equation (32), rather than equation (35), then the true \mathcal{C}^* would be given by a non-circular (and nontrivial) path through the saddle point. For small values of ϕ the leading terms in (32) will dominate and the factorization approximation (34) should be reliable. The circle will then provide a good approximation to \mathcal{C}^* in the vicinity of the saddle. For larger values of ϕ deviations can be anticipated as the fluctuations terms we have neglected, which at order i in the phase angle expansion (32) are proportional to $\langle N^i \rangle - \langle N \rangle^i$, become important. Moreover, the factorization approximation can be expected to break down close to any singular points in f which are intimately related to the growth of fluctuations. We will return to this point in detail in subsection III D, where we employ an exactly soluble model as a numerical testbed.

C. Asymptotic expansion of the canonical partition function

We now employ the steepest descents method to develop an asymptotic expansion for the canonical partition function. In all calculations from here on we will employ the circle approximation to the contour \mathcal{C}^* . Along this contour we can rewrite equation (13) as an integral over the phase-angle

$$Z_N = \frac{1}{2\pi x_0} \int_{-\pi}^{\pi} e^{Nf(x_0 e^{i\phi})} d\phi. \quad (38)$$

Taylor expanding f around the saddle, $\phi=0$, gives

$$Z_N = \frac{e^{Nf_0}}{2\pi} \int_{-\pi}^{\pi} d\varphi e^{N(\frac{1}{2!}x_0^2(e^{i\varphi}-1)^2 f_2 + \frac{1}{3!}x_0^3(e^{i\varphi}-1)^3 f_3 + \dots)}, \quad (39)$$

where we have used the shorthand notation

$$\frac{\partial f}{\partial x} = f^{(i)}(x_0) = f_i, \quad (40)$$

and where we note that $f_1 = 0$, since x_0 is a saddle point. We now Taylor expand the factors $(e^{i\varphi} - 1)$ in powers of φ to obtain the following expression

$$Z_N = \frac{e^{Nf_0}}{2\pi} \int_{-\pi}^{\pi} d\varphi e^{-\frac{1}{2}\kappa\varphi^2} \left(e^{iA\varphi^3 + B\varphi^4 + iC\varphi^5 + D\varphi^6 \dots} \right). \quad (41)$$

The first few coefficients appearing in the exponentials are given by

$$\begin{aligned} \kappa &= N\Lambda_2 & (42) \\ A &= N \left(-\frac{1}{2}\Lambda_2 - \frac{1}{6}\Lambda_3 \right) \\ B &= N \left(\frac{7}{24}\Lambda_2 + \frac{1}{4}\Lambda_3 + \frac{1}{24}\Lambda_4 \right) \\ C &= N \left(\frac{1}{8}\Lambda_2 + \frac{5}{24}\Lambda_3 + \frac{1}{12}\Lambda_4 + \frac{1}{120}\Lambda_5 \right) \\ D &= N \left(-\frac{31}{720}\Lambda_2 - \frac{1}{8}\Lambda_3 - \frac{13}{144}\Lambda_4 - \frac{1}{48}\Lambda_5 - \frac{1}{720}\Lambda_6 \right), \end{aligned}$$

where $\Lambda_i = x_0^i f^{(i)}(x_0)$. Finally, we Taylor expand the bracketed factor in the integrand of (41) to obtain a sum of simple integrals. Assuming that the integrand of each term decreases rapidly to zero as ϕ is increased away from $\varphi=0$ we extend the limits of integration and compute the resulting Gaussian integrals one by one. Observing that the coefficients (42) all scale linearly in N and that the Gaussian integrals scale as

$$\int_{-\infty}^{\infty} d\varphi \varphi^j e^{-\frac{1}{2}\kappa\varphi^2} \sim N^{-\frac{j}{2}} \quad (43)$$

for even values of the index j , we group the terms according to their dependence on N and thus obtain our

final expression for the asymptotic expansion

$$Z_N = \frac{e^{Nf_0}}{\sqrt{2\pi\kappa}} \left(1 + \frac{\alpha_1}{N} + \frac{\alpha_2}{N^2} + \dots \right), \quad (44)$$

where the α_i are independent of N . The first two of these coefficients are given by

$$\begin{aligned} \alpha_1 &= N \left(\frac{3B}{\kappa^2} - \frac{15A^2}{2\kappa^3} \right) & (45) \\ \alpha_2 &= N^2 \left(\frac{15D}{\kappa^3} + \frac{105}{\kappa^4} \left(\frac{B^2}{2} - AC \right) + \frac{945}{\kappa^5} \frac{A^2 B}{2} \right). \end{aligned}$$

Higher order terms become rapidly more complicated, but can be conveniently calculated using symbolic algebra software. Equation (44) enables approximate calculation of the canonical partition function for a finite system of N particles, provided that we have some expression (either exact or approximate) for the grand-canonical partition function.

Since equation (44) is an asymptotic expansion we anticipate that adding terms will first lead to a rapid convergence of the partial sum towards the exact value of Z_N . However, beyond a certain point, increasing the number of terms will degrade the numerical accuracy of the partial sum and lead eventually to a divergence. Optimal results are to be obtained by truncating the series at its ‘least term’ [14] and it may be hoped, but is by no means certain, that the optimal truncated series can be obtained before calculation of the coefficients α_i becomes impractical. A further complication is that the position of the least term within the series will not necessarily be the same for different values of N .

The asymptotic expansion of the canonical free energy follows by taking the logarithm of equation (44) and ordering terms according to their scaling with N . We thus obtain

$$\begin{aligned} F_N &= \Omega - \mu N + \frac{1}{2} k_B T \ln \left(2\pi \frac{\partial \langle N \rangle}{\partial \beta \mu} \right) \\ &+ k_B T \left(\frac{\alpha_1}{N} + \frac{(\alpha_2 - \frac{1}{2}\alpha_1^2)}{N^2} + \dots \right). \end{aligned} \quad (46)$$

In the thermodynamic limit the third term scales as $\ln(N)$ and so remains finite, but negligible in magnitude when compared to the first two terms, which are both extensive quantities. All higher-order terms vanish as $N \rightarrow \infty$. Equation (46) shows explicitly the emergence of the Legendre transform as a lowest-order approximation.

We note that the first three terms in equation (46) can already be found in a few scattered locations throughout the statistical mechanics literature (see e.g. [13]). The reason for this appears to be that these leading terms can be fortuitously obtained using two distinct approximations, both of which are convenient to implement but hard to justify. The first, and most dubious, of these consists of replacing the sum over particle number in equation (6) by an integral, thus blindly assuming that the sharp particle number N can be treated

as a continuous variable. This approach reproduces the zero-order term in equation (44), namely the prefactor $e^{Nf_0}/(2\pi a)^{\frac{1}{2}}$, and thus correctly captures the first three terms in equation (46), but generates erroneous higher-order terms. Further details of the ‘continuous N ’ approximation can be found in appendix B. The second, perhaps more reasonable, approach is to assume a linear path for evaluating the back transform (7). The integration is then performed in the imaginary direction along the path $\lambda = x_0 + iy$, implicitly assuming that the contribution from closing the path around some large loop around the origin does not contribute to the integral. As for the continuous N approximation, higher order terms in (46) are given incorrectly. This indicates that at order N^{-1} and beyond in (46) (equivalently, terms involving the α_i in equation (44)) are sensitive to the curvature of the contour \mathcal{C}^* . The circular contour identified in subsection III B correctly captures this curvature effect for the lowest order terms.

D. Yang-Lee zeros

Since the canonical partition functions are positive real numbers, the polynomial expression (6) for Ξ will have N_{\max} zeros which, by the ‘complex conjugate root theorem’ will appear in complex-conjugate pairs, removed from the real, positive axis (if N_{\max} is odd, then at least one of the roots will lie on the negative real axis). These are the famous Yang-Lee zeros of statistical mechanics, which encode important information about the phase behavior of the system [25, 26]. As the system size increases, the Yang-Lee zeros become more numerous and accumulate along well-defined curves in the complex plane. Using very general arguments Yang and Lee showed that if a zero approaches the real axis at fugacity x_c , then the system will undergo a phase transition at precisely this fugacity in the thermodynamic limit. The distribution of zeros in the complex plane and the way in which they approach the positive real axis on increasing N provides information about finite-size scaling and critical exponents [27, 28]. In recent work Peng *et al.* have shown that it is even possible to (indirectly) measure the location of the Yang-Lee zeros in experiment [29].

The success of the steepest descents method relies on the fundamental assumption that when integrating along the optimal contour \mathcal{C}^* the dominant contribution to the integral comes from the region around the saddle point. It is then assumed that a Taylor expansion of f about the saddle will yield a reasonable approximation to the integrand along the entire contour. However, since the function f depends on the logarithm of Ξ , see equation (14), it will clearly exhibit a divergence at each of the Yang-Lee zeros. These singular points impact the asymptotic evaluation of (7) in two distinct ways. Firstly, it is well-known that there is a close connection between the Yang-Lee zeros and fluctuations in particle number (c.f. the connection mentioned above between the zeros and criti-

cal exponents). The factorization approximation leading from equation (32) to equation (34) relies on neglecting fluctuations, $\langle N^n \rangle - \langle N \rangle^n \approx 0$, and can thus be expected to break down in the vicinity of a Yang-Lee singularity. This has the consequence that the true \mathcal{C}^* will deviate from the approximate circular form when approaching a singularity. Secondly, in the vicinity of a Yang-Lee zero a truncated Taylor expansion of the diverging function f will clearly be inadequate. The extent to which this problem is mitigated by deviations of the true \mathcal{C}^* away from Yang-Lee singularities remains an open question. We will return to this point when considering our numerical test-case in subsection IV B.

E. Asymptotic expansion for the one-body density

We next consider the asymptotic expansion of the one-body density. In this case the forwards transformation is given by an expression very similar to (6), namely

$$\Xi(\lambda)\rho(\mathbf{r}; \lambda) = \sum_{N=0}^{\infty} \lambda^N Z_N \rho_N(\mathbf{r}), \quad (47)$$

where ρ is the grand-canonical one-body density calculated at fugacity λ and ρ_N is the canonical one-body density for a system of strictly N particles.

Arguments analogous to those given in appendix A generate the following back-transform

$$Z_N \rho_N(\mathbf{r}) = \frac{1}{2\pi i} \oint_{\mathcal{C}^*} d\lambda \frac{\Xi(\lambda)\rho(\mathbf{r}; \lambda)}{\lambda^{N+1}}. \quad (48)$$

The procedure to deal with this integral closely follows that already presented in subsection III C. We first rewrite equation (48) in the following form

$$Z_N \rho_N(\mathbf{r}) = \frac{1}{2\pi i} \oint_C d\lambda \rho(\mathbf{r}; \lambda) \frac{e^{Nf(\lambda)}}{\lambda}. \quad (49)$$

Taylor expansion of f around the saddle point x_0 then yields

$$\rho_N(\mathbf{r}) Z_N = \frac{e^{Nf_0}}{2\pi} \int_{-\pi}^{\pi} d\phi \rho(\mathbf{r}; \lambda) e^{-\frac{1}{2}\kappa\phi^2} \times \left(e^{iA\phi^3 + B\phi^4 + iC\phi^5 + D\phi^6 \dots} \right), \quad (50)$$

where we have again used the circle approximation to the contour \mathcal{C}^* . We next perform a Taylor expansion of the grand-canonical density about the saddle point

$$\rho(\mathbf{r}; \lambda) = \rho(\mathbf{r}; x_0) + (\lambda - x_0) \left. \frac{\partial \rho(\mathbf{r}; \lambda)}{\partial \lambda} \right|_{x_0} + \frac{(\lambda - x_0)^2}{2} \left. \frac{\partial^2 \rho(\mathbf{r}; \lambda)}{\partial \lambda^2} \right|_{x_0} + \frac{(\lambda - x_0)^3}{6} \left. \frac{\partial^3 \rho(\mathbf{r}; \lambda)}{\partial \lambda^3} \right|_{x_0} + \dots \quad (51)$$

Insertion of the Taylor expansion

$$\begin{aligned} (\lambda - x_0) &= x_0(e^{i\phi} - 1) \\ &\approx x_0(i\phi + \frac{1}{2}(i\phi)^2 + \frac{1}{6}(i\phi)^3 + \dots), \end{aligned} \quad (52)$$

into equation (51) and then collecting powers of ϕ yields the phase angle expansion of the grand-canonical one-body density

$$\begin{aligned} \rho(\mathbf{r}; \lambda) &= \rho(\mathbf{r}; x_0) + ia(\mathbf{r})\phi + b(\mathbf{r})\phi^2 + ic(\mathbf{r})\phi^3 \\ &\quad + d(\mathbf{r})\phi^4 + ig(\mathbf{r})\phi^5 + h(\mathbf{r})\phi^6 + \dots, \end{aligned} \quad (53)$$

The position-dependent coefficients, a, b, \dots , are functions of derivatives of the grand-canonical density. The first few are given by

$$\begin{aligned} a(\mathbf{r}) &= P^{(1)}(\mathbf{r}), \\ b(\mathbf{r}) &= -\frac{1}{2} \left(P^{(1)}(\mathbf{r}) + P^{(2)}(\mathbf{r}) \right), \\ c(\mathbf{r}) &= -\frac{1}{6} \left(P^{(1)}(\mathbf{r}) + 3P^{(2)}(\mathbf{r}) + P^{(3)}(\mathbf{r}) \right), \\ d(\mathbf{r}) &= \frac{1}{24} \left(P^{(1)}(\mathbf{r}) + 7P^{(2)}(\mathbf{r}) + 6P^{(3)}(\mathbf{r}) + P^{(4)}(\mathbf{r}) \right), \end{aligned} \quad (54)$$

where we have defined

$$P^{(n)}(\mathbf{r}) = \left(x \frac{\partial}{\partial x} \right)^n \rho(\mathbf{r}) \Big|_{x=x_0} \quad (55)$$

Taylor expansion of the exponential containing the upper-case coefficients A, B, C, \dots in equation (50), using equation (53) and extending the range of integration yields a sum of Gaussian integrals. Regrouping the resulting terms according to their dependence on N we obtain our final form for the asymptotic expansion

$$\rho_N(\mathbf{r}) = \rho(\mathbf{r}; \lambda) + \frac{1}{Z_N} \frac{e^{Nf_0}}{\sqrt{2\pi\kappa}} \left(\frac{\Gamma_1(\mathbf{r})}{N} + \frac{\Gamma_2(\mathbf{r})}{N^2} + \dots \right), \quad (56)$$

where Z_N can be approximated by the asymptotic series (44). The first Γ coefficients are given by

$$\begin{aligned} \Gamma_1 &= N \left(\frac{b}{\kappa} - \frac{3aA}{\kappa^2} \right), \\ \Gamma_2 &= N^2 \left(\frac{3d}{\kappa^2} + \frac{15(bB - cA - aC)}{\kappa^3} - \frac{105(bA^2 + 2aAB)}{2\kappa^4} \right), \end{aligned} \quad (57)$$

where spatial arguments have been suppressed for conciseness. The calculation of higher-order coefficients is a straightforward but tedious exercise. Although not obvious from casual inspection of the expressions (57), the coefficients Γ_i all have spatial integral equal to zero. This property ensures the correct normalization of the asymptotic approximation (56) at any order of truncation.

As a final comment, we mention that the Yang-Lee zeros can be expected to play an equally important role for the asymptotic expansion of the one-body density as for the partition function, since both arise from essentially the same scheme.

F. Relation to the method of González

In the late 1990's González *et al.* derived the following expansion for the canonical density profile [3, 4]

$$\rho_N(\mathbf{r}) = \rho(\mathbf{r}) + g_1(\mathbf{r}) + g_2(\mathbf{r}) + \dots, \quad (58)$$

where the position-dependent terms g_i depend solely on grand-canonical input and scale with particle number $\sim N^{-i}$. The first two correction terms in equation (58) were found to be given by

$$g_1(\mathbf{r}) = -\frac{\langle (N - \langle N \rangle)^2 \rangle}{2} \frac{\partial^2 \rho(\mathbf{r})}{\partial \langle N \rangle^2}, \quad (59)$$

and

$$g_2(\mathbf{r}) = -\frac{\langle (N - \langle N \rangle)^2 \rangle}{2} \frac{\partial^2 g_1(\mathbf{r})}{\partial \langle N \rangle^2} - \frac{\langle (N - \langle N \rangle)^3 \rangle}{6} \frac{\partial^3 \rho(\mathbf{r})}{\partial \langle N \rangle^3}, \quad (60)$$

respectively (see equations 2.10 and 2.11 in Reference [4]). All grand-canonical quantities appearing on the right hand-side of (59) and (60) are evaluated at the fugacity for which $\langle N \rangle = N$ (identified as the saddle-point condition in our asymptotic approach). When truncated at order N^{-2} the expression (58) was shown to predict profiles for hard-spheres confined to a spherical cavity in good agreement with canonical Monte-Carlo simulation data. In appendix C we discuss the recursive back-substitution method used in References [3] and [4].

Following some algebra, the derivatives with respect to the average particle number and the fluctuation coefficients in equations (59) and (60) can be rewritten in terms of derivatives with respect to the fugacity. Further manipulation of the resulting expressions then reveals that equations (58), (59) and (60) derived by González *et al.* are, in fact, completely equivalent to the leading-order terms in the asymptotic expression (56) derived in the previous subsection. The recursive back-substitution method of González *et al.* thus reproduces the correct asymptotic expansion of the canonical one-body density to order N^{-2} . It seems to us a nontrivial observation that these earlier findings, calculated using a somewhat obscure recursive method, can only be reproduced when evaluating the back transform (7) along a sufficiently well chosen contour. Neither the *ad hoc* 'continuous N ' approximation nor the linear contour mentioned earlier can achieve this.

For the purpose of illustration we will briefly demonstrate the equivalence of the leading-order correction term, g_1 , to the term involving Γ_1 in equation (56). An analogous calculation, which we omit here as it is more lengthy but not more instructive, shows the equivalence of the second-order terms from the two approaches. We note that the work of González *et al.* makes no reference to a complex fugacity and thus all calculations presented for the remainder of this subsection are performed on the real axis, $\lambda = x$.

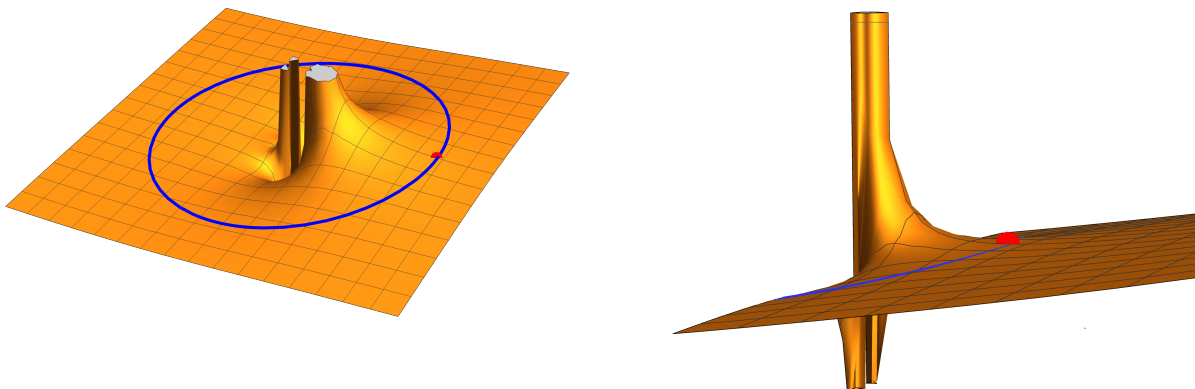


Figure 1. Visualizing the integrand of the back-transform, equation (7). **Left panel:** The quantity $\Re(\Xi/\lambda^{N+1})$ for $N = 3$ in the complex plane, highlighting the saddle point (Red point) and the circular contour we use in our calculations (blue curve) **Right panel:** The same surface viewed from a different angle to better view the saddle point.

We begin by rewriting g_1 using only derivatives with respect to x . This exercise in partial differentiation yields

$$g_1(\mathbf{r}) = -\frac{x}{2} \left(\frac{\partial \langle N \rangle}{\partial x} \right)^{-2} \left(\frac{d \langle N \rangle}{dx} \frac{d^2 \rho(\mathbf{r})}{dx^2} - \frac{d^2 \langle N \rangle}{dx^2} \frac{d \rho(\mathbf{r})}{dx} \right). \quad (61)$$

We next express the derivatives of $\langle N \rangle$ appearing in equation (61) in terms of derivatives of the function f . The required identities are

$$\left. \frac{\partial \langle N \rangle}{\partial x} \right|_{x_0} = N x_0 f^{(2)}(x_0), \quad (62)$$

$$\left. \frac{\partial^2 \langle N \rangle}{\partial x^2} \right|_{x_0} = N (x_0 f^{(3)}(x_0) + 2f^{(2)}(x_0)), \quad (63)$$

which follow from equations (10) and (14). The superscript on f indicates the n^{th} order derivative with respect to x . The correction term g_1 thus takes the form

$$g_1(\mathbf{r}) = -\frac{1}{2} \frac{1}{N f^{(2)}(x_0)} \left(\frac{\partial^2 \rho(\mathbf{r})}{\partial x^2} \right)_{x_0} + \frac{1}{2} \frac{x_0 f^{(3)}(x_0) + 2f^{(2)}(x_0)}{N x_0 (f^{(2)}(x_0))^2} \left(\frac{\partial \rho(\mathbf{r})}{\partial x} \right)_{x_0}. \quad (64)$$

On the other hand, the leading-order correction term in our asymptotic expansion (56) is given by

$$\frac{1}{Z_N} \frac{e^{N f_0}}{\sqrt{2\pi\kappa}} \frac{\Gamma_1}{N} = \frac{1}{Z_N} \frac{e^{N f_0}}{\sqrt{2\pi\kappa}} \left(\frac{b}{\kappa} - \frac{3aA}{\kappa^2} \right). \quad (65)$$

From equation (44) we have, to leading order, that the canonical partition function is given by

$$Z_N = \frac{e^{N f_0}}{\sqrt{2\pi\kappa}}. \quad (66)$$

Direct substitution of the above expression for Z_N as well as the expressions for a, b and A into (65) exactly reproduces equation (64). We have thus shown that the g_1 term in the expansion of González *et al.* is equivalent to the leading-order correction term of our asymptotic expansion.

IV. APPLICATION TO 1D HARD-RODS

We will next investigate the asymptotic expressions obtained above using an exactly soluble model, namely hard-rods in one spatial dimension, confined between two hard-walls. For this system the canonical partition functions and thus (via equation (6)) the grand-canonical partition function are given by simple analytic expressions. For the one-body density, exact grand-canonical profiles can be calculated by variational minimization of the Percus hard-rod free-energy functional [7, 30]. Application of exact matrix inversion then yields the canonical profile for all values of N [8]. The one-dimensional confined rod model is thus a rare case for which we have a complete and exact description of the thermodynamics and one-body density in both the canonical and grand-canonical ensembles.

The canonical partition function of N rods confined between two hard walls separated by a distance L is given exactly by

$$Z_N = \frac{1}{N!} (L - N)^N, \quad (67)$$

where we have set both the thermal wavelength and the rod length equal to unity. The corresponding grand-canonical partition function is then given by the definition (6) and can be directly evaluated for any complex value of the fugacity.

N	x_0	Z_N^{exact}	$Z_N^{(1)}$	ε_1	$Z_N^{(2)}$	ε_2
1	0.240534	5.9	6.39083	7.68%	6.20258	4.87%
2	0.760902	12.005	12.4889	3.87%	11.4915	4.27%
3	2.16724	9.8865	10.1417	2.51%	9.46997	4.21%
4	7.8077	2.9470	3.00396	1.89%	3.0228	2.50%
5	66.3881	0.2063	0.206539	0.11%	0.309272	33.2%

Table I. Data for a system of six hard-rods confined between hard walls with separation $L=6.9$. We give the saddle point fugacity, x_0 , the exact partition function, Z_N , and both the first- and second-order asymptotic approximation, $Z_N^{(1)}$ and $Z_N^{(2)}$, respectively. The percentage error of these approximations is given by $\varepsilon_{1,2}$. Data for the maximally packed state $N=6$ are omitted, since the results are not reliable.

Grand-canonical density profiles can be determined by solving the Euler-Lagrange equation (4) using the following exact expression for the excess Helmholtz free energy

$$F^{ex}[\rho] = -k_B T \int_{-\infty}^{\infty} n_0(x) \ln(1 - n_1(x)) dx \quad (68)$$

where the weighted densities n_0 and n_1 are generated from the convolution integrals

$$n_\alpha(x) = \int_{-\infty}^{\infty} \rho(x') w_\alpha(|x - x'|) dx', \quad (69)$$

with geometrically-based weight functions given by

$$w_0(x) = \frac{1}{2} (\delta(x - R) + \delta(x + R)) \quad (70)$$

$$w_1(x) = \begin{cases} 1, & \text{if } -R < x < R \\ 0, & \text{otherwise,} \end{cases} \quad (71)$$

where $R=1/2$ in our chosen units of length. Calculating grand-canonical profiles at N_{\max} different values of the fugacity enables the definition (47) to be cast as a matrix multiplication. Numerical inversion then yields all canonical density profiles, ρ_N , for $N = 1, \dots, N_{\max}$, as described in Reference [8].

Let us now choose a specific and representative example by fixing $L = 6.9$. Due to this confinement the system can admit at most six rods and the grand partition function (6) is a finite polynomial. For each value of N we can determine exactly the corresponding canonical partition function Z_N using (67) as well as the position of the saddle point x_0 using the saddle condition (16), see the values given in Table I. We note that the fugacity of the saddle point corresponding to the most densely packed state, namely $\langle N \rangle = 6$, is so large that it is practically unattainable by numerical minimization of the grand potential.

A. Numerical results: Partition function

We begin with a quick visual inspection the integrand of equation (7), namely the function Ξ/λ^{N+1} . Despite

the many applications of saddle-point approximation in the physical and mathematical literature, it is exceedingly rare to find actual visualizations of the saddle for any concrete problem. We thus show in Fig. 1 a surface plot of the real part of the integrand in the complex plane for the case $N=3$. As anticipated, we indeed observe a saddle point on the real axis, which is located at $x_0 = 2.167$ and indicated in the Figure by a red dot. The blue curve shows the approximate circular contour we employ in our calculations.

Table I gives the asymptotic approximation to the canonical partition functions, obtained from equation (44), together with their exact values and the location of the saddle points. For $N \leq 5$ truncation at first-order provides a good approximation to the exact value of Z_N , with an error which decreases with increasing N . This is the behavior one would expect from a valid asymptotic expansion. The results to second-order are, however, less satisfactory and, with the exception of the case $N = 1$, degrade the accuracy of the approximation. We suspect that already at second-order the output of the theory becomes sensitive to the choice of contour and that the approximate circular contour is already insufficient to generate the true second order terms which would result from employing the optimal contour \mathcal{C}^* . In the following subsection we will analyse these contour differences in more detail, but they are closely connected with the presence of Yang-Lee zeros.

A well-known property of asymptotic series is that increasing the number of terms generates partial sums which initially converge towards the exact result but, beyond a certain point, begin to diverge as further terms are added [14]. Truncation at the so-called ‘least term’ provides an optimal approximation (although further improvements can still be made [31]). This suggests an alternative interpretation of the data in Table I, namely that the asymptotic series has reached its least term already at first-order and that this then represents the optimal truncation.

B. Yang-Lee zeros and the optimal contour

For the hard-rod system under consideration we find that all six Yang-Lee zeros are located on the negative real axis in the complex λ -plane (which is consistent with earlier studies [32, 33]). Their locations are listed in Table II, where we observe that the distance of the zeros from the origin increases very rapidly as the maximally packed state ($N=6$) is approached. In Figure 2 we plot

x_1^{YL}	x_2^{YL}	x_3^{YL}	x_4^{YL}	x_5^{YL}	x_6^{YL}
-0.404	-0.545	-0.940	-2.304	-10.728	-264.172

Table II. For a system of six hard-rods confined between two hard walls with separation $L = 6.9$ all six Yang-Lee zeros lie on the negative real axis in the complex fugacity plane.

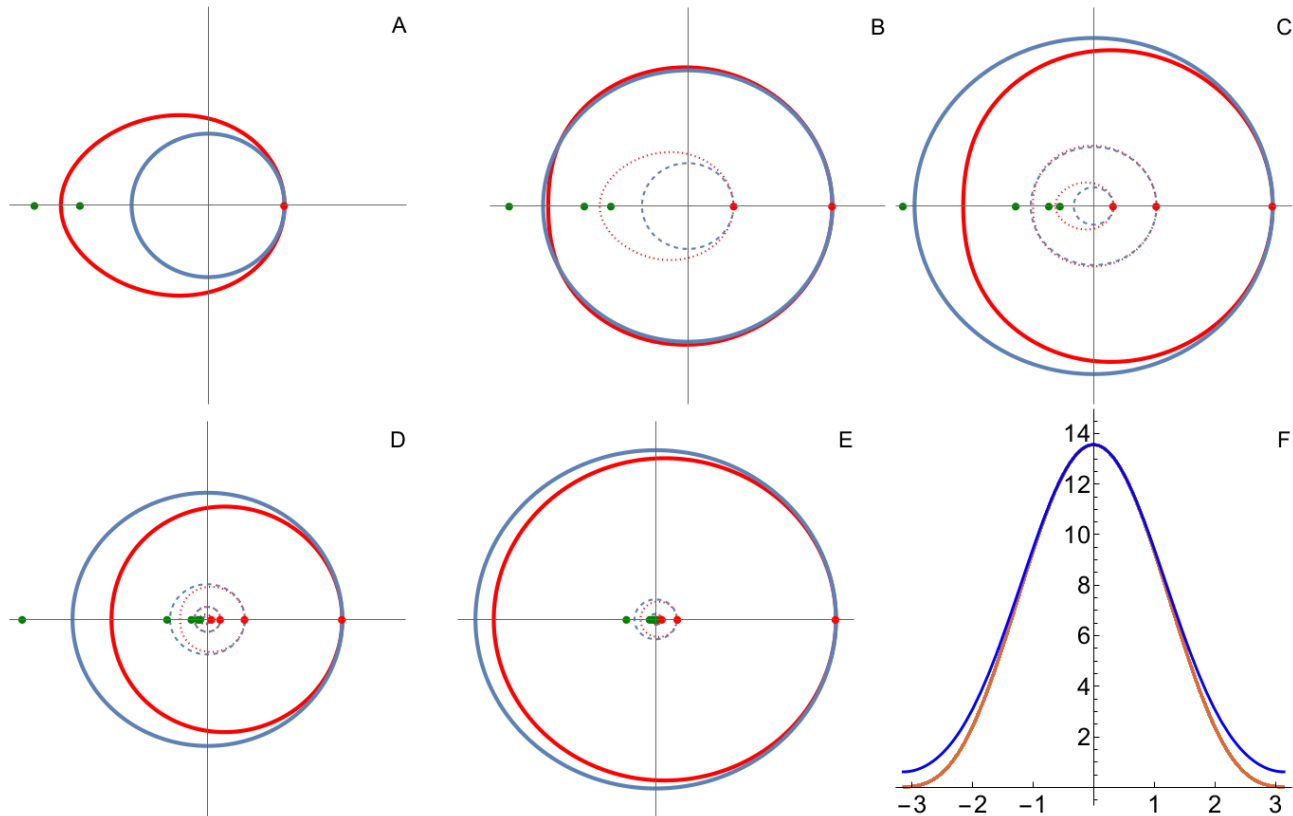


Figure 2. Figures A to E show the true optimal contour \mathcal{C}^* (red) and the approximate circular contour (blue) for (A) $N=1$, (B) $N=2$, (C) $N=3$, (D) $N=4$, (E) $N=5$, in the complex fugacity plane. Red dots represent the saddle points, and green dots represent Yang-Lee zeroes. The dotted and dashed curves in each of the Panels (B)-(E) simply show the contours from the preceding Panels for visual reference as we zoom out. For small phase-angles the two contours show good agreement but then deviate as the Yang-Lee zeros are approached. Note how the true optimal contour deforms to enclose exactly N Yang-Lee zeros. Figure (F) shows $\exp(Nf_{re})$ for the case $N=1$ along both the true contour (red) and the circular contour (blue).

both the Yang-Lee zeros and the saddle points, together with the approximate circular contour (blue curve) and the true optimal contour (red curve). The latter was obtained by starting from the saddle point and then numerically solving the equation $f_{im} = 0$ to track a path through the complex λ -plane.

For small values of the phase angle, ϕ , the true contour is well approximated by the circle, as might have been anticipated by comparing the exact equation (32) with the approximate form (34). As the value of ϕ is increased the fluctuation terms, $\langle N^i \rangle - \langle N \rangle^i$, neglected in equation (34) begin to play an increasingly important role and the true contour deviates from the circular form. We observe that the true contour always seems to deform in such a way that it threads neatly between the Yang-Lee zeros in an attempt to maintain as much distance as possible from these singular points. Somewhat more mysteriously, the true contour for any given N deforms to enclose precisely N Yang-Lee zeros. This behaviour, which is most clearly visible for the case $N=1$, suggests a deep connection between the saddle points, the Yang-Lee zeros and the topology of the zero-phase contour \mathcal{C}^* .

It seems to us very likely that the deviations of the circular contour from the true optimal contour are responsible for the disappointing performance of the second-order asymptotic truncation detailed in Table I. Focusing on the case $N=1$ we plot in Panel (F) the function $e^{Nf_{re}}$, which is the key part of the integrand in equation (24). Although the circular contour provides a reasonable approximation to $e^{Nf_{re}}$, deviations are clearly visible as the negative real axis is approached. This corresponds to the range of phase-angles for which the true contour deforms to avoid the singularity in f arising from the first Yang-Lee zero. We recall that the circular contour originates from application of the factorization approximation to the exact series (32) and thus implicitly assumes that fluctuations are negligible. Since the Yang-Lee zeros are associated with increased particle-number fluctuations the assumptions underlying the circle approximation can be expected to break down close to these singular points. This suggests that the (nontrivial) relation between the positions of the saddle points on the positive real axis and the Yang-Lee zeros on the negative real axis can have a significant effect on the accuracy of the circle

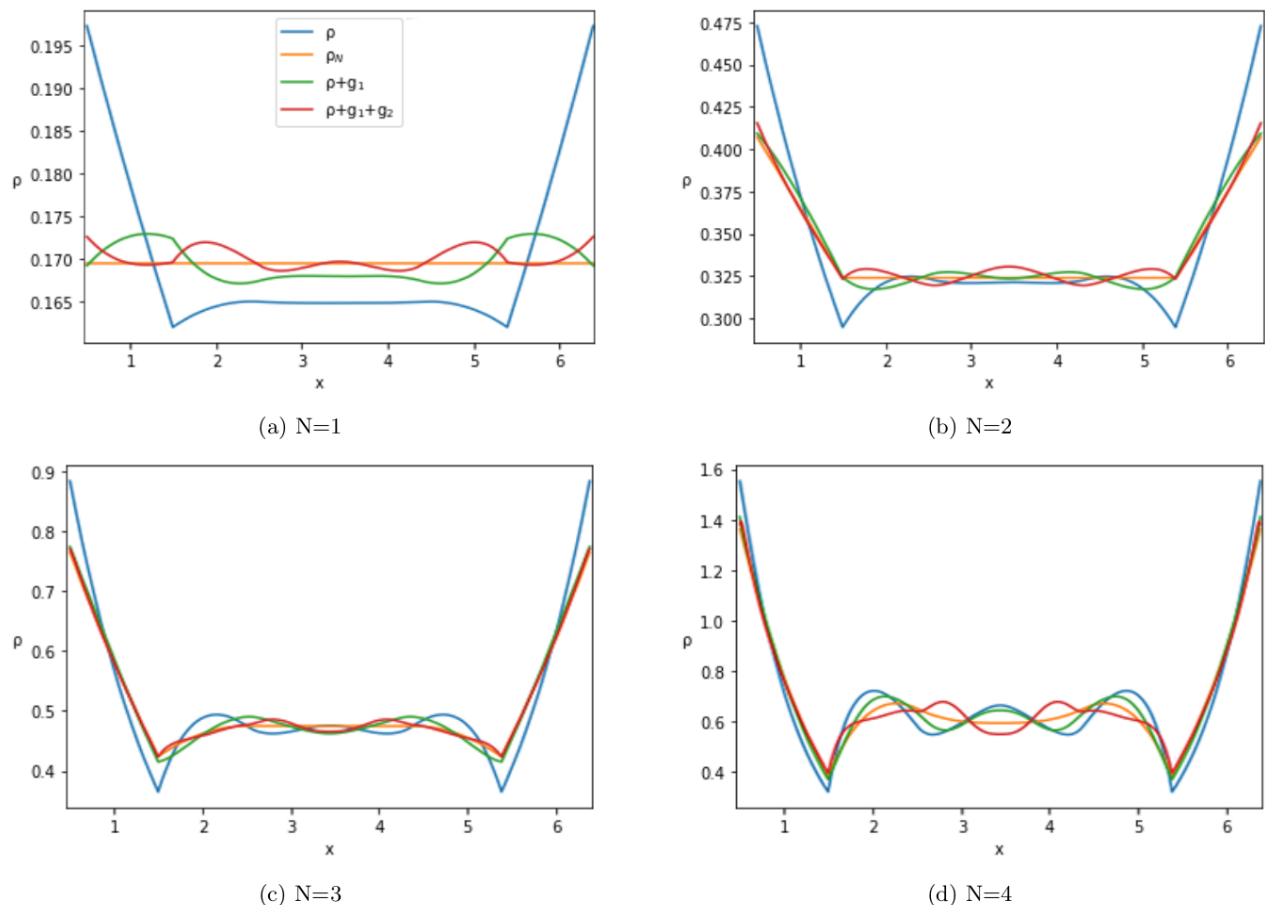


Figure 3. Density profiles for hard-rods confined between two hard walls with separation $L = 6.9$. The maximal number of rods which can fit in the slit is $N_{\max} = 6$. Profiles are shown for the cases $N = 1, \dots, 4$. For larger values of N the performance degrades and we encounter a high-packing breakdown of the asymptotic expansion. The first-order term provides clearly corrects the most serious deficiencies of the grand-canonical profiles, whereas the second order term fails to provide a convincing systematic improvement.

approximation. Specifically, if $x_0 \approx |x_i^{\text{YL}}|$ for any value of i , then the approximate circular contour will pass close to the zero and will thus be unlikely to provide a good account of the true contour.

The simplicity of the hard-rod model restricts the Yang-Lee zeros to the negative real axis and, although their influence is not negligible, they are sufficiently distant from the saddle points that the asymptotic method can still be applied with reasonable success. More realistic model fluids with attractive interparticle interactions will certainly present a more complicated pattern of zeros. For example, simply adding a square-well nearest-neighbour attraction to the hard-rod model is sufficient to move the zeros off the negative real axis [32, 33]. A clear implication of our findings is that a nontrivial distribution of zeros over the complex fugacity plane would seriously complicate determination of an appropriate contour. It therefore seems unlikely that the simple circle approximation would be sufficient to correctly determine even the leading-order terms in the asymptotic expansion for attractive systems.

C. Numerical results: One-body density

For three-dimensional hard-spheres confined within a spherical cavity González *et al.* obtained accurate profiles using the first two terms in the expansion (56) (equation (58) when written in their notation); results which we have indeed verified using our own independent codes. For some special packing configurations one of the spheres can be quite tightly localized at the center of the cavity (quasi-0D states) due to interactions with its surrounding neighbours. These situations were found to have strongly ensemble-dependent density profiles and were thus used to test the convergence of the approximate canonical expansion. Although the first-order correction already gave a good account of canonical Monte-Carlo simulation data, it remained uncertain that the addition of the second-order term could provide a systematic improvement over the first-order results [4].

The present model system of confined hard-rods presents a more demanding test of the asymptotic

method than the three-dimensional cavity, since ensemble differences are more pronounced and the packing constraints on the particles are more restrictive. In Figure 3 we investigate the predictions of the asymptotic approximation to the one-body density for particle numbers $N = 1, \dots, 4$. The blue curves are the exact grand-canonical profiles, calculated by solving the Euler-Lagrange equation (4) using the functional (68), whereas the orange curves show the exact canonical profiles we seek to approximate. The green and red curves then give the asymptotic results to first- and second-order, respectively, corresponding to using the Γ_1 and Γ_2 terms of equation (56) (equivalently, the g_1 and g_2 terms in the González expansion (58)).

We begin by discussing the extreme case of a single rod, $N = 1$. In Panel (a) of Figure 3 we observe a large difference between the (trivial) canonical density profile and the grand-canonical profile obtained from DFT. The latter contains unwanted contributions from particle number fluctuations and thus exhibits unphysical packing structure. Despite the fact that $N = 1$ is certainly not a large value of N the asymptotic method performs better than one might expect and shows clear evidence of convergence towards the exact canonical result. Although the asymptotic approximation introduces unphysical oscillations, these both reduce in amplitude and snake more tightly around the exact solution in going from first- to second-order. A similar trend is visible in Panels (b)-(d). We note that the ‘contact regions’ of the density profiles, $0.5 < x < 1.5$ and $5.4 < x < 6.4$, are very well approximated by the asymptotic expansion, whereas the central region exhibits a slower convergence. This behaviour is particularly apparent for the case $N = 4$, where addition of the second-order correction term only marginally improves on the first-order prediction. These general trends are fully consistent with the three-dimensional results of González *et al.* who observed that convergence of the density profiles was more rapid close to the boundaries than in the center of the cavity.

For $N = 5$ and 6 we encounter difficulties to obtain reasonable profiles from the asymptotic expansion. First indications of this breakdown are already apparent in the slower convergence of the partial sums for the case $N = 4$ (shown in Panel (d) of Figure 3) and become much worse as maximal packing is approached. A similar breakdown at large cavity packings was observed by González *et al.* (see page 3684 of Reference [4]). It appears that the asymptotic expansion of canonical quantities for confined fluids is subject to two competing mechanisms. On the one hand increasing the value of N initially leads to improved convergence, as would be expected from an asymptotic series. On the other hand as the value of N approaches N_{\max} a second mechanism becomes relevant and leads to the high-packing breakdown. The consequence is that the expansion exhibits a ‘sweet spot’ at intermediate values of N , for which our expressions perform best. The origin of the breakdown and its relation to the choice of contour remains an open question.

V. DISCUSSION AND CONCLUSIONS

We have developed the method of asymptotics to address the problem of calculating the thermodynamics and microstructure of confined fluids in the canonical ensemble. Although by no means the first attempt in this direction we think that our formulation clearly exposes the fundamental mechanisms determining the success or failure of the method, all of which are ultimately related to the presence of Yang-Lee zeros. Indeed, it is difficult to imagine making the connection between asymptotic series and the Yang-Lee zeros from either the recursive back-substitution method of González *et al.* [3, 4] or direct matrix inversion [8], since these approaches do not involve the complex fugacity plane in which the zeros are to be found.

Our chosen test-system of one-dimensional hard rods provides a good illustration the main issues, since for this model the Yang-Lee zeros are sufficiently removed from the saddle points that their influence is not overly dramatic, but still significant enough that we can draw some general conclusions. In other words, the zeros make their presence felt, but not to the extent that they completely invalidate the approximations we have employed, as could well be the case for systems with more realistic interaction potentials. Moreover, the fact that the hard rod system is exactly soluble removes any confusion which could arise when using approximate grand-canonical input; interpretation of the asymptotic series is already complicated enough. Nevertheless, the interaction of grand-canonical input error with the asymptotics of the back-transform surely remains both an interesting and necessary topic for future study.

One-dimensional hard rods do not exhibit a bulk phase transition, which is reflected in the fact that the Yang-Lee zeros for this model all lie along the negative real axis in the complex fugacity plane. For systems with a bulk phase transition this will no longer be the case and the presence of nontrivial zeros off the real axis will pose serious challenges for the asymptotic method. Even if the location of the zeros could be identified, then this would still leave open the dual problem of determining the optimal steepest descents contour and then actually performing the required integration along it. Phase transitions are characterized by a thermodynamic limit which takes different analytic forms in distinct regions of thermodynamic parameter space. We thus suspect that the Stokes phenomena will become an important part of the picture; the form of the asymptotic expansion changes discontinuously as a thermodynamic parameter (e.g. the complex fugacity) moves across a Stokes (or anti-Stokes) line [34–36]. This behaviour is a consequence of approximating an analytic function using simpler multivalued functions. It seems likely that the Yang-Lee zeros will turn out to be located on some type of Stokes line which separates different forms of the asymptotic expansion as the thermodynamic limit is approached. Investigations into this potentially rich phenomenology are underway.

Finally, we mention that an analogous asymptotic approach can be employed to back-transform canonical observables to the microcanonical ensemble. In this case the required contour integral is performed in the plane of complex inverse-temperature, β , and phase transitions are manifest as zeros in the complex β plane [37]. These so-called Fisher zeros approach the positive real axis in the thermodynamic limit in much the same way as the Yang-Lee zeros in the present study. It is thus clear that the Fisher zeros will influence the choice of a suitable integration contour and thereby affect the form of any asymptotic expansion.

ACKNOWLEDGMENTS

We would like to thank S. M. Tschopp for insightful comments and stimulating discussions.

Appendix A: Contour integral for obtaining the canonical partition functions

The inverse transform (7) is a special case of the well-known Cauchy integral. To demonstrate the validity of (7) we substitute the definition of the grand partition function (6) into the contour integral. This yields

$$2\pi i Z_N = \oint_C \frac{d\lambda}{\lambda^{N+1}} + \oint_C \frac{Z_1}{\lambda^N} d\lambda + \dots \quad (\text{A1})$$

$$\dots + \oint_C \frac{Z_{N-1}}{\lambda^2} d\lambda + \oint_C \frac{Z_N}{\lambda} d\lambda + \oint_C Z_{N+1} d\lambda + \dots$$

All terms have an integrand of the form Z_j/λ^α , where we recall that the canonical partition functions do not depend on λ . The simplest and most convenient choice of contour enclosing the origin is a circle of radius x_0 . Using the parameterization $\lambda = x_0 e^{i\phi}$ gives $d\lambda = ix_0 e^{i\phi} d\phi = i\lambda d\phi$. Each term in the expansion then involves an integral of the following form

$$\oint_C \frac{d\lambda}{\lambda^\alpha} = i \int_0^{2\pi} d\phi \lambda^{1-\alpha} \quad (\text{A2})$$

$$= ix_0^{(1-\alpha)} \int_0^{2\pi} d\phi e^{i\phi(1-\alpha)}.$$

This integral yields zero, unless the exponent in the exponential vanishes. We thus conclude that

$$\oint_C \frac{Z_j}{\lambda^\alpha} d\lambda = \begin{cases} 2\pi i Z_j, & \text{if } \alpha = 1 \\ 0, & \text{otherwise.} \end{cases} \quad (\text{A3})$$

Inserting this result into (A1) produces the identity, thus proving the inverse formula (7). The integral operator

$$\frac{1}{2\pi i} \oint_C d\lambda \frac{1}{\lambda^{N+1}}, \quad (\text{A4})$$

which depends on the parameter N , thus acts on Ξ to extract the term Z_N from the sum (6).

Appendix B: Treating N as a continuous variable

Occasionally in the statistical mechanics literature one finds a vague description of how to invert equation (6) by replacing the discrete sum over N with a continuum integral. The reason for the enduring appeal of this suspicious scheme is that it rather easily generates the first three terms in the asymptotic expansion of the Helmholtz free energy (although higher-order terms are incorrect). In the following we give some details of this ‘continuous N ’ approximation.

Using the standard relation $F_N = -k_B T \ln(Z_N)$, where F_N is the true canonical Helmholtz free energy for fixed particle number, we can rewrite equation (6) in the following form

$$\Xi = \sum_{N=0}^{\infty} e^{\beta\mu N - \beta F_N}. \quad (\text{B1})$$

If we now close our eyes and simply replace the sum by an integral we obtain

$$\Xi = \int_0^{\infty} dN e^{-\mu\beta(-N + \frac{1}{\mu} F_N)}, \quad (\text{B2})$$

where we have factored-out the chemical potential in the exponent so that it can be treated as a large parameter. Since non-integer values of N are not physical the status of equation (B2) is obviously questionable.

To apply Laplace’s method we first rewrite the integral (B2) in the standard form

$$\Xi = \int_0^{\infty} dN e^{-\mu g(N)} \quad (\text{B3})$$

where we have defined

$$g(N) = \beta \left(-N + \frac{F_N}{\mu} \right). \quad (\text{B4})$$

Setting $dg/dN = 0$ locates the saddle point, which corresponds to setting $\langle N \rangle = N$. Taylor expansion of the exponent in equation (B3) around the saddle and truncating at second-order then yields the approximation

$$\Xi \approx e^{\beta(\mu\langle N \rangle - F_N)} \int_0^{\infty} dN e^{(N - \langle N \rangle)^2 \beta F_N^{(2)}}$$

$$= e^{\beta(\mu\langle N \rangle - F_N)} \sqrt{\frac{2\pi}{\beta F_N^{(2)}}} \quad (\text{B5})$$

where $F_N^{(2)}$ is the second derivative of F_N with respect to the ‘continuous’ variable N . The saddle condition implies the standard canonical relation

$$\mu = \left. \frac{\partial F_N}{\partial N} \right|_{N=\langle N \rangle}. \quad (\text{B6})$$

Substitution into equation (B5) then gives the following approximation to the grand partition function

$$\Xi \approx e^{\beta(\mu\langle N \rangle - F_N)} \sqrt{2\pi \frac{\partial \langle N \rangle}{\partial \beta \mu}}. \quad (\text{B7})$$

Taking the logarithm yields

$$\ln(\Xi) \approx \langle N \rangle \mu \beta - \beta F_N + \frac{1}{2} \ln \left(2\pi \frac{\partial \langle N \rangle}{\partial \beta \mu} \right), \quad (\text{B8})$$

which, after trivial rearrangement, yields the final approximation to the Helmholtz free energy

$$F_N = \Omega - \mu N + \frac{1}{2} k_B T \ln \left(2\pi \frac{\partial \langle N \rangle}{\partial \beta \mu} \right). \quad (\text{B9})$$

We thus recover the first three terms in the asymptotic expansion (46).

Appendix C: The González expansion method

In the late 1990's González *et al.* developed a scheme to approximate the canonical one-body density profile using grand-canonical input quantities obtained from DFT. The following derivation is our interpretation of that given in References [3, 4]. We hope that this does justice to the original work and that it clarifies any possible points of confusion.

The starting point of the approach is to write the grand-canonical one-body density as a weighted sum of canonical one-body densities

$$\rho(\mathbf{r}) = \sum_{N=0}^{\infty} \rho_N(\mathbf{r}) P(N; \lambda), \quad (\text{C1})$$

where $P(N)$ is the probability to find N particles at (real) fugacity λ . Equation (C1) is simply a rewriting of equation (47) in the main text. For a given value of λ the average particle number is

$$\langle N \rangle = \sum_{N=0}^{\infty} N P(N; \lambda). \quad (\text{C2})$$

Before proceeding further we find it useful to identify a hypothetical one-body density, $\tilde{\rho}_N$. This is a generalized canonical one-body density for which N is viewed as a continuous variable. For integer values of N it coincides with the true canonical density. Let us now rewrite equation (C1) using this new density

$$\rho(\mathbf{r}) = \sum_{N=0}^{\infty} \tilde{\rho}_N(\mathbf{r}) P(N; \lambda). \quad (\text{C3})$$

The introduction of, $\tilde{\rho}$, represents the most uncertain aspect of the procedure presented here, since it is not a well-defined statistical mechanical quantity for non-integer values of N . However, this step seems to be necessary to generate a useful recursive scheme.

We next Taylor expand the $\tilde{\rho}$ about the chosen value of

$\langle N \rangle$ in powers of the continuous variable N . This yields

$$\rho(\mathbf{r}) = \sum_{N=0}^{\infty} P(N; \lambda) \left(\tilde{\rho}_{\langle N \rangle}(\mathbf{r}) + (N - \langle N \rangle) \frac{\partial \tilde{\rho}_N(\mathbf{r})}{\partial N} \Big|_{\langle N \rangle} + \frac{1}{2} (N - \langle N \rangle)^2 \frac{\partial^2 \tilde{\rho}_N(\mathbf{r})}{\partial N^2} \Big|_{\langle N \rangle} + \dots \right). \quad (\text{C4})$$

where the partial derivatives on the right-hand side are evaluated at $N = \langle N \rangle$ and $\tilde{\rho}_{\langle N \rangle} \equiv \tilde{\rho}_{N=\langle N \rangle}$. Performing the sum in equation (C4) then gives

$$\rho(\mathbf{r}) = \tilde{\rho}_{\langle N \rangle}(\mathbf{r}) + \frac{1}{2} \langle (N - \langle N \rangle)^2 \rangle \frac{\partial^2 \tilde{\rho}_N(\mathbf{r})}{\partial N^2} \Big|_{\langle N \rangle} + \frac{1}{6} \langle (N - \langle N \rangle)^3 \rangle \frac{\partial^3 \tilde{\rho}_N(\mathbf{r})}{\partial N^3} \Big|_{\langle N \rangle} + \dots \quad (\text{C5})$$

We seek to find the first term on the right hand side of equation (C5). Trivial rearrangement yields

$$\tilde{\rho}_{\langle N \rangle}(\mathbf{r}) = \rho(\mathbf{r}) - \frac{1}{2} \langle (N - \langle N \rangle)^2 \rangle \frac{\partial^2 \tilde{\rho}_N(\mathbf{r})}{\partial N^2} \Big|_{\langle N \rangle} - \frac{1}{6} \langle (N - \langle N \rangle)^3 \rangle \frac{\partial^3 \tilde{\rho}_N(\mathbf{r})}{\partial N^3} \Big|_{\langle N \rangle} + \dots \quad (\text{C6})$$

We next assume that we can make the replacement

$$\frac{\partial^n \tilde{\rho}_N(\mathbf{r})}{\partial N^n} \Big|_{N=\langle N \rangle} = \frac{\partial^n \rho_{\langle N \rangle}(\mathbf{r})}{\partial \langle N \rangle^n} \Big|_{\langle N \rangle=N} \quad (\text{C7})$$

which indeed seems plausible, but is surely difficult to justify in any rigorous way. We thus generate the following expansion

$$\rho_{\langle N \rangle}(\mathbf{r}) = \rho(\mathbf{r}) - \frac{1}{2} \langle (N - \langle N \rangle)^2 \rangle \frac{\partial^2 \rho_{\langle N \rangle}(\mathbf{r})}{\partial \langle N \rangle^2} \Big|_{\langle N \rangle=N} - \frac{1}{6} \langle (N - \langle N \rangle)^3 \rangle \frac{\partial^3 \rho_{\langle N \rangle}(\mathbf{r})}{\partial \langle N \rangle^3} \Big|_{\langle N \rangle=N} - \dots, \quad (\text{C8})$$

Equation (C8) forms the basis for an iterative back-substitution scheme (termed ‘formal inversion’ in the original papers of González *et al.*). Recursive substitution of the entire right-hand side of (C8) into the partial derivatives then produces the main result, equation (58), given in the main text.

It is quite remarkable to us that this recursive scheme successfully generates the leading terms of an asymptotic expansion, despite not having an obvious connection to the asymptotic evaluation of any integral. The deeper reasons for why our systematic expansion (56) coincides with the González expression, at least for the terms we could check, will require further investigation and at present remains obscure. As a final comment we mention that the González derivation does not offer much insight into when and why the expansion may fail. As far as we can see this information can only be gained by analyzing the grand-canonical to canonical transform in the complex fugacity plane.

-
- [1] T. L. Hill, *J. Chem. Phys.* **36**, 3182 (1962).
- [2] T. L. Hill, *Thermodynamics of small systems* (Dover, New York, 2013).
- [3] A. González, J. A. White, F. L. Román, S. Velasco, and R. Evans, *Phys. Rev. Lett.* **79**, 2466 (1997).
- [4] A. González, J. A. White, F. L. Román, and R. Evans, *J. Chem. Phys.* **109**, 3637 (1998).
- [5] A. Stradner, H. Sedgewick, F. Cardinaux, W. Poon, S. Egelhaaf, and P. Schurtenberger, *Nature* **432**, 492 (2004).
- [6] R. Evans, *Advances in Physics* **28**, 143 (1979).
- [7] R. Evans, Ch. 3 in *Fundamentals of Inhomogeneous Fluids*, D. Henderson, ed., Marcel Dekker, New York (1992).
- [8] D. de las Heras and M. Schmidt, *Phys. Rev. Lett.* **113**, 238304 (2014).
- [9] J. Reinhardt and J. M. Brader, *Phys. Rev. E* **85**, 011404 (2012).
- [10] J. A. White, A. González, F. L. Román, and S. Velasco, *Phys. Rev. Lett.* **84**, 1220 (2000).
- [11] J. A. White and S. Velasco, *Phys. Rev. E* **62**, 4427 (2000).
- [12] J. J. Salacuse, A. R. Denton, and P. A. Egelstaff, *Phys. Rev. E* **53**, 2382 (1996).
- [13] J. L. Lebowitz and J. K. Percus, *Phys. Rev.* **122**, 1675 (1961).
- [14] R. Dingle, *Asymptotic expansions: Their derivation and interpretation* (Academic Press, London, 1973).
- [15] F. W. J. Olver, *Asymptotics and Special Functions* (Academic Press, London, 1974).
- [16] C. M. Bender and S. A. Orszag, *Advanced Mathematical Methods for Scientists and Engineers* (McGraw-Hill, New York, 1978).
- [17] A. Cohen, *Numerical methods for Laplace transform inversion* (Springer, New York, 2007).
- [18] R. Fowler, *Statistical Mechanics* (Cambridge University Press, 1936).
- [19] R. Kubo, *Statistical Mechanics* (Elsevier, 1990).
- [20] E. Schrödinger, *Statistical thermodynamics* (Cambridge University Press, 1948).
- [21] K. Huang, *Statistical Mechanics* (Wiley, 1963).
- [22] M. Boas, *Mathematical methods in the physical sciences* (Wiley, 1966).
- [23] P. Morse and H. Feshbach, *Methods of theoretical physics: Part 1* (McGraw Hill, New York, 1953).
- [24] J. Matthews and R. Walker, *Mathematical methods of physics* (Benjamin, New York, 1971).
- [25] C. N. Yang and T. D. Lee, *Phys. Rev.* **87**, 404 (1952).
- [26] T. D. Lee and C. N. Yang, *Phys. Rev.* **87**, 410 (1952).
- [27] I. Bena, M. Droz, and A. Lipowski, *International Journal of Modern Physics B* **19**, 4269 (2005).
- [28] A. Deger and C. Flindt, *Phys. Rev. Res.* **1**, 023004 (2019).
- [29] X. Peng, H. Zhou, B.-B. Wei, J. Cui, J. Du, and R.-B. Liu, *Phys. Rev. Lett.* **114**, 010601 (2015).
- [30] J. K. Percus, *J. Stat. Phys.* **15**, 505.
- [31] M. V. Berry and C. J. Howls, *Proc. Roy. Soc. A* **430**, 653 (1990).
- [32] T. Niemeyer, *Physics Letters* **29A**, 231 (1969).
- [33] T. Niemeyer and A. Weijland, *Physica* **50**, 457 (1970).
- [34] G. G. Stokes, *Acta Mathematica* **26**, 393 (1902).
- [35] M. V. Berry, *Proc. Roy. Soc. A* **422**, 7 (1989).
- [36] M. V. Berry, *Publ. Math. Inst. Hautes Études Sci.* **68**, 211 (1989).
- [37] M. E. Fisher, in *Statistical Physics, Weak Interactions, Field Theory, Lectures in Theoretical Physics*, ed. W. E. Brittin (University of Colorado Press, Boulder, 1965).